Hepatic metal ion transporter ZIP8 regulates manganese homeostasis and manganese-dependent enzyme activity

Wen Lin,[1] David R. Vann,[2] Paschalis-Thomas Doulias,[3] Tao Wang,[1] Gavin Landesberg,[4] Xueli Li,[5] Emanuela Ricciotti,[6] Rosario Scalia,[4] Miao He,[5,7] Nicholas J. Hand,[8] and Daniel J. Rader[1,6,8]

[1]Department of Medicine, Perelman School of Medicine, and [2]Department of Earth and Environmental Science, School of Arts and Sciences, University of Pennsylvania, Philadelphia, Pennsylvania, USA.
[3]Children's Hospital of Philadelphia Research Institute and Department of Pharmacology, Children's Hospital of Philadelphia and University of Pennsylvania, Philadelphia, Pennsylvania, USA.
[4]Department of Physiology, Temple University, Philadelphia, Pennsylvania, USA. [5]Palmieri Metabolic Disease Laboratory, Children's Hospital of Philadelphia, Philadelphia, Pennsylvania, USA.
[6]Institute for Translational Medicine and Therapeutics, [7]Department of Pathology and Laboratory Medicine, Perelman School of Medicine, and [8]Department of Genetics, Perelman School of Medicine, University of Pennsylvania, Philadelphia, Pennsylvania, USA.

Genetic variants at the solute carrier family 39 member 8 (*SLC39A8*) gene locus are associated with the regulation of whole-blood manganese (Mn) and multiple physiological traits. *SLC39A8* encodes ZIP8, a divalent metal ion transporter best known for zinc transport. Here, we hypothesized that ZIP8 regulates Mn homeostasis and Mn-dependent enzymes to influence metabolism. We generated *Slc39a8*-inducible global-knockout (ZIP8-iKO) and liver-specific–knockout (ZIP8-LSKO) mice and observed markedly decreased Mn levels in multiple organs and whole blood of both mouse models. By contrast, liver-specific overexpression of human ZIP8 (adeno-associated virus–ZIP8 [AAV-ZIP8]) resulted in increased tissue and whole blood Mn levels. ZIP8 expression was localized to the hepatocyte canalicular membrane, and bile Mn levels were increased in ZIP8-LSKO and decreased in AAV-ZIP8 mice. ZIP8-LSKO mice also displayed decreased liver and kidney activity of the Mn-dependent enzyme arginase. Both ZIP8-iKO and ZIP8-LSKO mice had defective protein N-glycosylation, and humans homozygous for the minor allele at the lead *SLC39A8* variant showed hypogalactosylation, consistent with decreased activity of another Mn-dependent enzyme, β-1,4-galactosyltransferase. In summary, hepatic ZIP8 reclaims Mn from bile and regulates whole-body Mn homeostasis, thereby modulating the activity of Mn-dependent enzymes. This work provides a mechanistic basis for the association of *SLC39A8* with whole-blood Mn, potentially linking *SLC39A8* variants with other physiological traits.

Introduction

Common genetic variants at the solute carrier family 39 member 8 (*SLC39A8*) genomic locus are significantly associated genome wide with whole-blood manganese (Mn) (1) as well as a variety of other traits and diseases, including blood pressure (2, 3), HDL cholesterol (HDL-C) (4, 5), BMI (6), and schizophrenia (7, 8). Importantly, the lead variant for blood Mn and all of the other traits is a coding variant, rs13107325 (Ala391Thr), that has an 8% minor allele frequency in people of European ancestry (9) and has been reported to encode a protein with reduced function (10, 11). This variant is also an expression quantitative trait locus (eQTL) for *SLC39A8* in human liver and is associated with lower hepatic *SLC39A8* expression (4, 6). However, the mechanisms underlying the associations of *SLC39A8* with blood Mn levels and other human physiological traits remain unknown.

SLC39A8 encodes a protein known as ZIP8, a divalent metal ion transporter best known for its ability to transport zinc (Zn) (12). It has also been shown in vitro to transport Mn (13), iron (Fe) (14), and cadmium (Cd) (13), with higher affinity for Mn than for Zn in mammalian cells (13). Hypomorphic *Slc39a8* mice exhibited diminished tissue Zn and Fe levels, stunted growth, multiple-organ hypoplasia, anemia, and perinatal death (15). Patients carrying *SLC39A8* mutations had severe Mn deficiency, neurological and skeletal defects, and biomarkers of type II congenital disorders of glycosylation (CDG) (16–18), a growing family of genetic diseases that affect multiple organs and systems (19). However, there is virtually nothing known about how ZIP8 regulates metal ion metabolism in vivo.

Mn is an essential trace nutrient and a cofactor for numerous enzymes (20). These Mn-dependent enzymes encompass all 6 major enzyme families, in addition to several Mn metalloenzymes that contain tightly bound Mn ion(s) (20). Two of the best-known Mn-dependent enzymes are arginase and b-1,4-galactosyltransfearse, which require Mn for catalytic activity (21, 22). Mn deficiency impairs bone formation, fertility, and the metabolism of glucose, lipids, and carbohydrates (20, 23). Despite the essentiality of Mn, only divalent metal transporter 1 (*DMT1*) (24, 25) and *SLC30A10* (25, 26) have been established as Mn transporters in vivo, and the physiological regulation of Mn metabolism is not well understood.
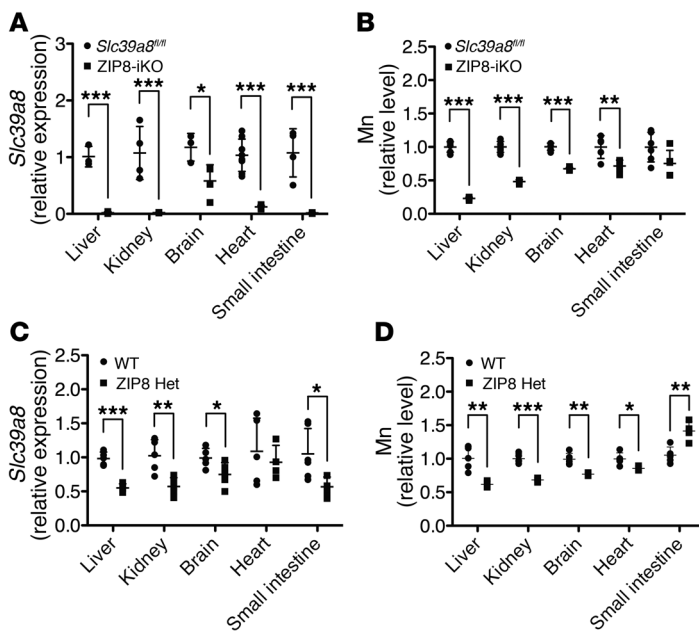
We hypothesized that ZIP8 regulates Mn homeostasis and therefore plays important roles in metabolism via the regulation of Mn-dependent enzymes. To test this hypothesis, we generat-

Figure 1. Global *Slc39a8* deletion leads to systemic Mn deficiency. (**A**) qPCR analysis of *Slc39a8* expression in male *Slc39a8^{fl/fl}* and ZIP8-iKO mice injected with tamoxifen at 8 weeks of age and sacrificed 5 weeks after the injection (*n* = 3–6). (**B**) ICP-OES analysis of Mn levels in male *Slc39a8^{fl/fl}* and ZIP8-iKO mice injected with tamoxifen at 8 weeks of age and sacrificed 5 weeks after injection (*n* = 5–6). (**C**) qPCR analysis of *Slc39a8* expression in 12- to 14-week-old male WT and ZIP8 Het mice (*n* = 4–6). (**D**) ICP-OES analysis of Mn levels in 12- to 14-week-old male WT and ZIP8 Het mice (*n* = 4–5). qPCR results were normalized to *Gapdh*. ICP-OES results were normalized to wet tissue weight. Mn levels in the tissues were normalized to the average of the control group. Data on the absolute Mn content can be found in the Supplemental Table. All data represent the mean ± SD. ***$P \leq 0.001$, **$P \leq 0.01$, and *$P \leq 0.05$, by Student's *t* test.

ed *Slc39a8*-inducible global-knockout mice (referred to hereafter as ZIP8-iKO mice) and liver-specific–knockout mice (referred to hereafter as ZIP8-LSKO mice) and also overexpressed *SLC39A8* in the liver (adeno-associated virus–ZIP8 [AAV-ZIP8]). Our studies establish hepatic ZIP8 as a regulator of whole-body Mn homeostasis through reclamation of Mn from bile; through this mechanism, ZIP8 regulates the activity of the Mn-dependent enzymes arginase and β-1,4-galactosyltransferase.

Results

Inducible global Slc39a8 deletion leads to systemic Mn deficiency. SLC39A8 is widely expressed (12). To study the physiological effects of ZIP8 deficiency, we generated inducible global *Slc39a8*–knockout mice by crossing conditional floxed *Slc39a8* (*Slc39a8^{fl/fl}*) mice with *UBC-CreERT2*–transgenic mice. *Slc39a8* deletion was induced by tamoxifen injection. Quantitative PCR (qPCR) analysis revealed that, compared with control *Slc39a8^{fl/fl}* mice injected with tamoxifen, *Slc39a8^{fl/fl} UBC-CreERT2* mice (hereafter referred to as ZIP8-iKO mice) injected with tamoxifen had efficient *Slc39a8* deletion in the liver (–98%, *P* < 0.001), kidney (–98%, *P* < 0.001), brain (–51%, *P* = 0.034), heart (–88%, *P* < 0.001), and small intestine (–98%, *P* < 0.001) (Figure 1A). Despite the known ability of ZIP8 to transport Zn and Fe, tissue Zn and Fe levels were not different in ZIP8-iKO mice compared with levels in controls (Supplemental Figure. 1, A and B). In contrast, tissue Mn levels in ZIP8-iKO mice were markedly reduced. Compared with control mice, Mn levels were decreased in the liver (–77%, *P* < 0.001), kidney (–52%, *P* < 0.001), brain (–31%, *P* < 0.001), and heart (–27%, *P* = 0.008) of ZIP8-iKO mice (Figure 1B). This observation is consistent with the findings that patients carrying *SLC39A8* mutations develop severe deficiency of Mn but not Zn, that *SLC39A8* variants are associated with whole-blood Mn but not Zn, and that ZIP8 has high affinity for Mn but not Zn in mammalian cells. We compared HDL-C levels and body weights of ZIP8-iKO mice with those of the control mice on

a chow or Western diet and observed no significant differences. We did not observe overt neurological or skeletal abnormalities in the ZIP8-iKO mice.

Consistent with the systemic Mn deficiency seen in ZIP8-iKO mice, *Slc39a8* heterozygous mice (hereafter referred to as ZIP8 Het mice), which had decreased *Slc39a8* expression in the liver (–44%, *P* < 0.001), kidney (–44%, *P* = 0.006), and brain (–24%, *P* = 0.04) (Figure 1C), also had significantly decreased Mn levels in these organs, though to a lesser extent than in the ZIP8-iKO mice. In ZIP8 Het mice, Mn levels were reduced by 39% in the liver (*P* = 0.003), 32% in the kidney (*P* < 0.001), 23% in the brain (*P* = 0.002), and 14% in the heart (*P* = 0.021) (Figure 1D); in contrast, Mn levels were increased by 34% in the small intestine (*P* = 0.004), despite decreased *Slc39a8* expression in this organ (–51%, *P* = 0.014).

Hepatic ZIP8 regulates whole-body Mn homeostasis. The liver plays a vital role in regulating Mn homeostasis in vivo (27). In order to determine the contribution of hepatic ZIP8, we generated *Slc39a8* liver-specific–knockout mice by crossing *Slc39a8^{fl/fl}* mice with *Alb-Cre*–transgenic mice. Compared with control *Slc39a8^{fl/fl}* mice, *Slc39a8^{fl/fl} Alb-Cre* mice (hereafter referred to as ZIP8-LSKO mice) had decreased *Slc39a8* mRNA levels in the liver (–75%, *P* < 0.001) but normal *Slc39a8* expression in other tissues (Figure 2A). Mn levels were not only substantially decreased in the liver (–69%, *P* < 0.001), but also in the kidney (–49%, *P* < 0.001), brain (–34%, *P* < 0.001), and heart (–47%, *P* < 0.001), indicating that hepatic *Slc39a8* deletion decreased systemic tissue Mn levels (Figure 2B). To confirm that the regulation of Mn by *Slc39a8* is not specific to male mice, we examined Mn levels in the liver and kidney of female ZIP8-LSKO mice and also observed decreased Mn compared with levels in the control mice (–76%, *P* < 0.001 for liver and –57%, *P* < 0.001 for kidney) (Supplemental Figure 2; supplemental material available online with this article; https://doi.org/10.1172/JCI90896DS1). In addition, whole-blood Mn was decreased in
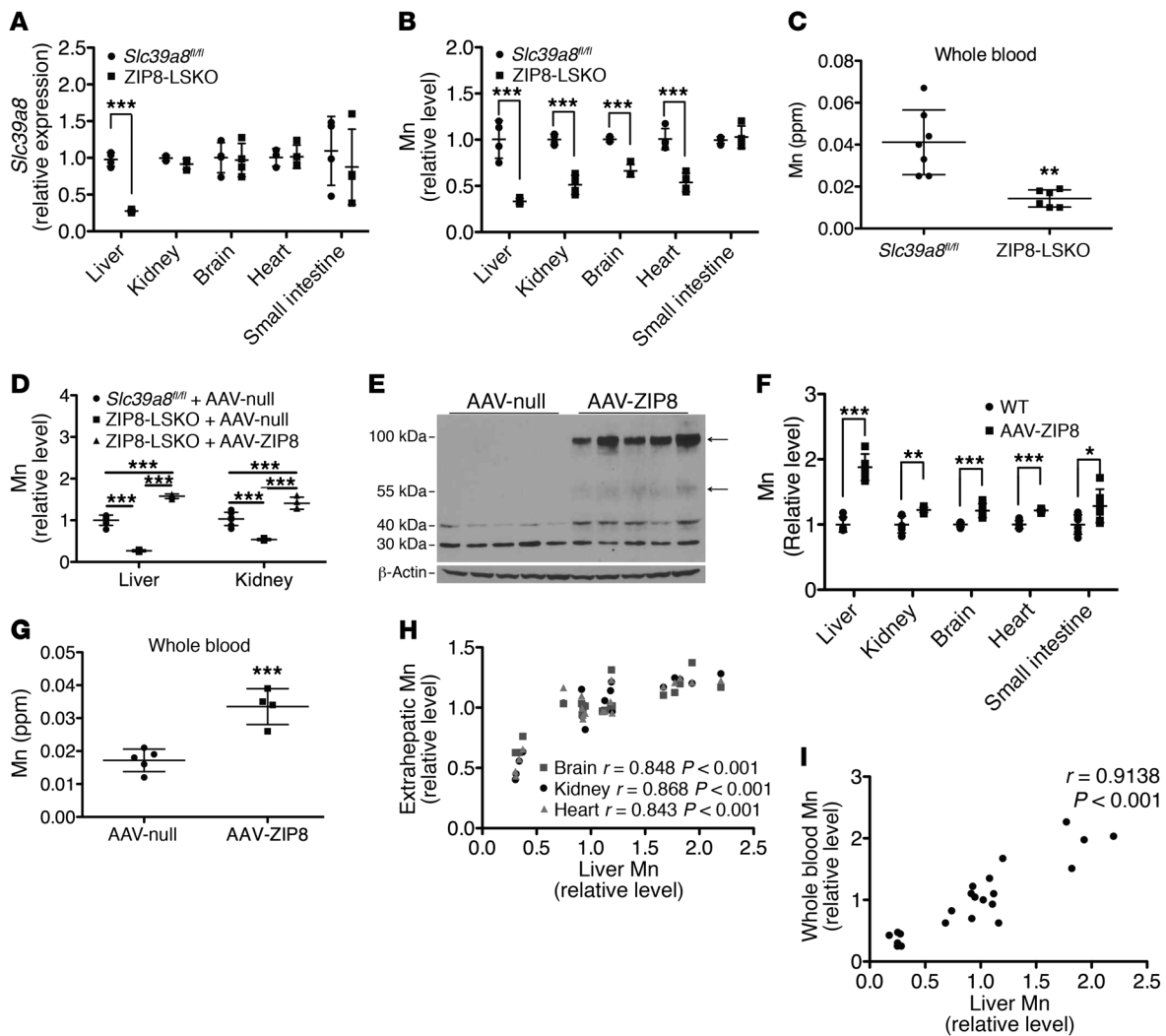
Figure 2. Hepatic ZIP8 regulates whole-body Mn homeostasis. (**A**) qPCR analysis of *Slc39a8* expression in 12- to 14-week-old male *Slc39a8*^fl/fl and ZIP8-LSKO mice (*n* = 3–4). (**B**) ICP-OES analysis of Mn levels in 12- to 14-week-old male *Slc39a8*^fl/fl and ZIP8-LSKO mice (*n* = 4). (**C**) ICP-MS analysis of Mn levels in the whole blood of 14- to 16-week-old male *Slc39a8*^fl/fl and ZIP8-LSKO mice (*n* = 7 and 6, respectively). (**D**) ICP-OES analysis of Mn levels in 12- to 14-week-old male *Slc39a8*^fl/fl mice injected with AAV-null and in ZIP8-LSKO mice injected with AAV-null or AAV-ZIP8 (*n* = 3–6). (**E**) Western blot analysis of ZIP8 in liver lysates of male B6 mice injected with AAV-null or AAV-ZIP8 at 10 weeks of age and sacrificed 4 weeks after injection. Arrows indicate the ZIP8 bands. (**F**) ICP-OES analysis of Mn levels in male B6 mice injected with AAV-null or AAV-ZIP8 at 10 weeks of age and sacrificed 4 weeks after injection (*n* = 6). (**G**) ICP-MS analysis of Mn levels in the whole blood of male B6 mice injected with AAV-null or AAV-ZIP8 at 8 weeks of age and sacrificed 4 weeks after injection (*n* = 5 and 4, respectively). qPCR results were normalized to *Gapdh*. ICP-OES results were normalized to wet tissue weight. Mn levels were normalized to the average of the control group. Data on the absolute Mn content can be found in the Supplemental Table. (**A**–**C**, **F**, and **G**) Comparisons between 2 groups were performed using Student's *t* test. Multiple comparisons in **D** were performed using 1-way ANOVA and Tukey's multiple comparisons test. ****P* ≤ 0.001, ***P* ≤ 0.01, and **P* ≤ 0.05. (**H**) Correlation analysis between hepatic Mn and Mn levels in the kidney, brain, and heart of WT and ZIP8-LSKO mice and AAV-null– and AAV-ZIP8–injected B6 mice (*n* = 19). (**I**) Correlation analysis between hepatic Mn and Mn levels in the whole blood of WT and ZIP8-LSKO mice and AAV-null– and AAV-ZIP8–injected B6 mice (*n* = 22). Mn levels were normalized to the average of the control group. The results in **H** and **I** were analyzed by Pearson's test. All data are shown as the mean ± SD.

ZIP8-LSKO mice (−65%, *P* = 0.002) (Figure 2C). As with the ZIP8-iKO mice, compared with controls, the ZIP8-LSKO mice exhibited no significant differences in HDL-C or body weight and no overt neurological or skeletal abnormalities.

In order to test whether human ZIP8 could compensate for the absence of murine ZIP8, we injected an AAV vector expressing human *SLC39A8* under the control of a liver-specific promoter (hereafter referred to as AAV-ZIP8) into ZIP8-LSKO mice. Expression of human ZIP8 in liver restored Mn levels in the liver and kidney (Figure 2D).

To determine whether hepatic expression of human *SLC39A8* regulates whole-body Mn homeostasis over a wider range of expression levels, we injected WT mice with AAV-ZIP8. Human *SLC39A8* mRNA was only detectable in the liver and not other tissues (data not shown). Western blot analysis confirmed that AAV-ZIP8 mice expressed human ZIP8 protein in the liver (Figure 2E). Mn levels were significantly increased in the liver (+87%, *P* < 0.001), kidney (+22%, *P* = 0.002), brain (+21%, *P* < 0.001), heart (+22%, *P* < 0.001), and small intestine (+28%, *P* = 0.04) (Figure 2F), indicating that liver-specific human ZIP8 overexpression increased systemic tissue Mn levels.
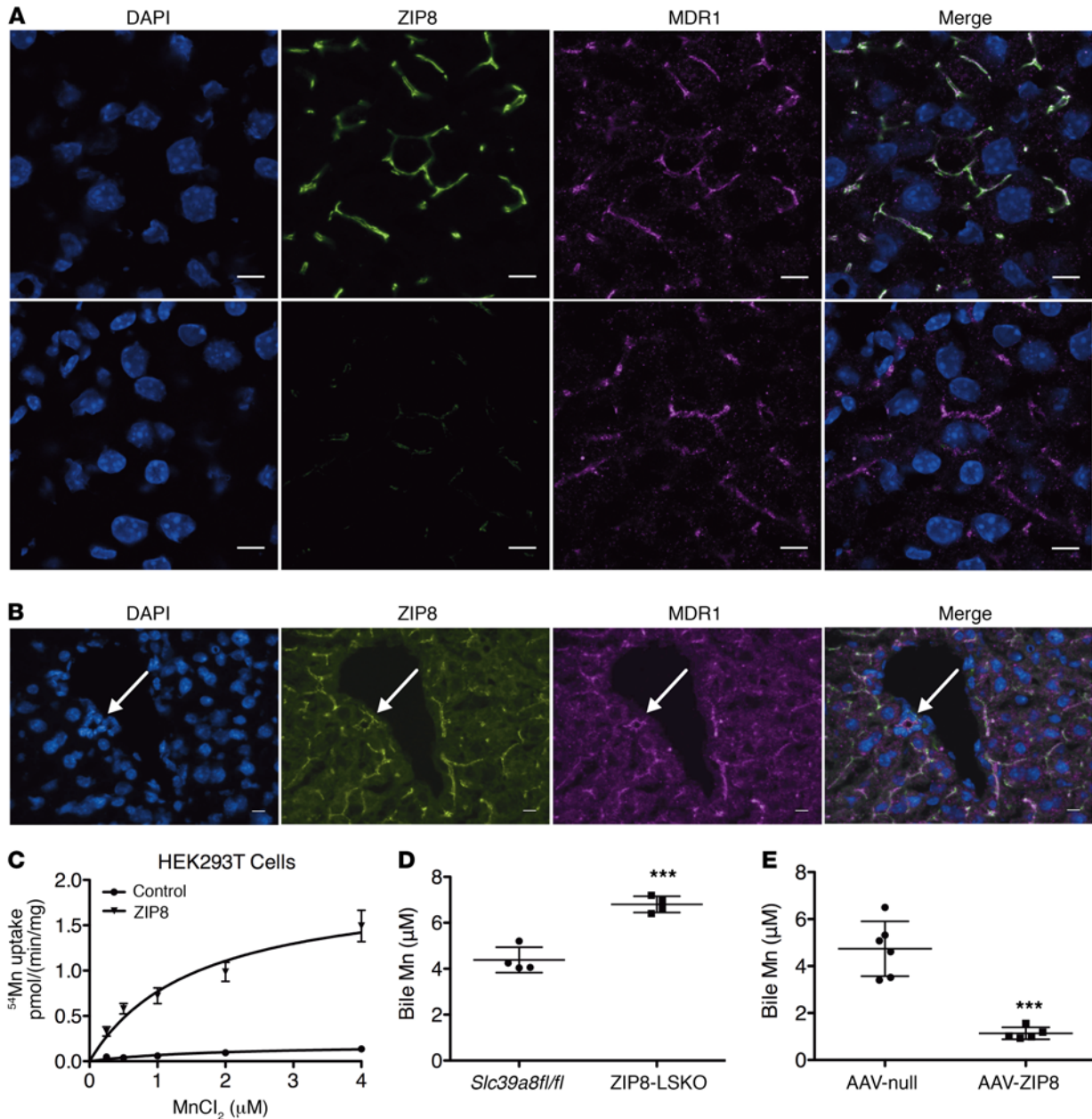
Figure 3. ZIP8 reclaims Mn from the bile. (**A** and **B**) Immunofluorescence analysis of ZIP8 (green) and MDR1 (magenta) localization in *Slc39a8^fl/fl* and ZIP8-LSKO mouse liver sections. Arrows indicate bile ducts. Results are representative of 3 independent experiments. (**C**) ^{54}Mn uptake study of HEK293T cells overexpressing human ZIP8 (*n* = 3). (**D**) ICP-MS analysis of Mn levels in the bile of 12- to 14-week-old male *Slc39a8^fl/fl* and ZIP8-LSKO mice (*n* = 4). (**E**) ICP-MS analysis of Mn levels in the bile of male B6 mice injected with AAV-null or AAV-ZIP8 at 10 weeks of age and sacrificed 4 weeks after injection (*n* = 6 and 5, respectively). Scale bars: 10 μm. All data are shown as the mean ± SD. ***$P \leq 0.001$, **$P \leq 0.01$, and *$P \leq 0.05$, by Student's *t* test.

Mn was also increased in the whole blood (+94%, $P < 0.001$) (Figure 2G). Neither Zn nor Fe levels were changed in the tissues (Supplemental Figure 1, C–F) or whole blood (Supplemental Figure 3) of ZIP8-LSKO or AAV-ZIP8 mice compared with the corresponding controls.

We examined the correlation between hepatic Mn and Mn levels in the kidney, brain, heart, small intestine, and whole blood using data generated from these experiments. There was a linear correlation between hepatic Mn and Mn levels in the kidney ($r = 0.8677$, $P < 0.001$), brain ($r = 0.8483$, $P < 0.001$), heart ($r = 0.8427$, $P < 0.001$) (Figure 2H), and whole blood ($r = 0.9138$, $P = 0.001$) (Figure 2I). These results provided evidence that hepatic expression of ZIP8

specifically and quantitatively regulates whole-body homeostasis of Mn, but not Zn or Fe, over a wide range of expression levels.

ZIP8 reclaims Mn from the bile. ZIP family members are known to import metal ions into the cytosol, and previous studies showed that mouse ZIP8 promoted the uptake of Mn in fetal fibroblasts (13) and kidney proximal tubule cells (28). We tested the ability of human ZIP8 to promote the uptake of Mn into mammalian cells. Expression of human ZIP8 in HEK293T cells resulted in substantially increased cellular Mn uptake (Figure 3C), confirming its role in cellular Mn uptake. The major route of Mn disposal is biliary excretion, whereby hepatocytes export Mn across the apical

membrane into bile canaliculi (29, 30). We hypothesized that ZIP8 is localized to the hepatocyte apical canalicular membrane and functions to reclaim Mn from the bile by promoting its reuptake into hepatocytes. Immunofluorescence analysis of mouse liver sections revealed that ZIP8 was colocalized with multiple drug resistance–associated protein (MDR1), a canalicular marker, in WT hepatocytes and was undetec in hepatocytes from ZIP8-LSKO mice (Figure 3A). We also detected ZIP8 on the apical membrane of cholangiocytes, the columnar epithelial cells of the bile duct, where it may further reclaim Mn from the bile (Figure 3B). Consistent with our model, ZIP8-LSKO mice had increased Mn in the bile (+55%, $P < 0.001$) (Figure 3D), despite reduced levels of Mn in liver and other tissue, and AAV-ZIP8 mice had decreased Mn in the bile (–76%, $P < 0.001$) (Figure 3E), despite increased levels of Mn in liver and other tissue. Zn and Fe levels were not changed in the bile of ZIP8-LSKO or AAV-ZIP8 mice (Supplemental Figure 4). These observations combined strongly support a model in which ZIP8 is localized to the apical surface of the hepatocyte and reclaims Mn (but not Zn or Fe) from the bile, reducing the biliary excretion of Mn and defending whole-body Mn stores.

ZIP8 acts through Mn to quantitatively modulate arginase activity. Arginase is a Mn-dependent enzyme that binds Mn in the catalytic site and requires Mn for catalytic activity. ZIP8-LSKO mice had a significant decrease in hepatic arginase activity, which was rescued by liver-specific overexpression of human ZIP8 using AAV (Figure 4A). We found that hepatic arginase activity was also decreased in female ZIP8-LSKO mice (–60%, $P < 0.001$) (Supplemental Figure 5A), as well as in male ZIP8-iKO and ZIP8 Het mice (–47%, $P < 0.001$ and –25%, $P = 0.009$, respectively) (Supplemental Figure 5, B and C). Conversely, AAV-ZIP8 mice, which had increased hepatic Mn, had increased hepatic arginase activity (+67%, $P < 0.001$) (Figure 4B). In both ZIP8-LSKO and AAV-ZIP8 mice, arginase protein levels, as determined by Western blotting, were not changed (Figure 4C), indicating a change in the specific activity of the protein.

Preincubation of pooled WT and ZIP8-LSKO liver lysates ex vivo with increasing concentrations of $MnCl_2$ revealed that the addition of Mn progressively increased arginase activity until reaching a plateau (Figure 4, D and E). Examination of the relative arginase activity under each $MnCl_2$ concentration revealed that hepatic arginase activity in the ZIP8-LSKO mice was lower than in WT mice, without added Mn, but was restored to the same level as that in WT mice at a $MnCl_2$ concentration of 250 μM or higher (Figure 4F). Similar experiments with liver lysates from individual animals confirmed that 250 μM $MnCl_2$ increased hepatic arginase activity in both WT and ZIP8-LSKO mice and eliminated their difference (Figure 4G). Thus, Mn added ex vivo rescues the defective arginase activity in livers from ZIP8-LSKO mice.

Our correlation analyses using data from all mouse models revealed a very strong and significant linear correlation between hepatic Mn levels and hepatic arginase activity ($r = 0.9558$, $P < 0.001$) (Figure 4H). ZIP8-LSKO mice, which had decreased Mn levels in the kidney (–40%, $P = 0.001$) (Figure 4I), consistent with the previous experiment shown in Figure 2, also had significantly decreased arginase activity in the kidney (–20%, $P = 0.002$) (Figure 4J). Furthermore, in kidneys from liver-specific–knockout mice, arginase activity linearly correlated with Mn levels ($r = 0.8570$, $P = 0.0015$) (Figure 4K). Thus, tissue Mn content is a

quantitative regulator of tissue arginase activity over a wide range of Mn concentrations. Taken together, our results demonstrate that hepatic ZIP8 acts to maintain tissue Mn homeostasis, which in turn modulates arginase activity, not only in the liver but in extrahepatic tissues as well.

ZIP8 acts through Mn to modulate protein N-glycosylation. β-1,4-Galactosyltransferase is a Mn-dependent enzyme that requires Mn for substrate binding and catalytic activity. It catalyzes the transfer of galactose to the glycan moiety of protein during protein N-glycosylation (31), while Mn deficiency has been found to impair protein N-glycosylation, especially galactosylation (32). Moreover, patients carrying *SLC39A8* mutations have severe Mn deficiency and defective protein N-glycosylation, with prominent hypogalacto-sylation (16–18). We examined N-glycan profiles in the serum of our *Slc39a8*-knockout mouse models using MALDI/time-of-flight mass spectrometric (MALDI-TOF-MS) analysis (Figure 5, A–D). Compared with control mice, we observed that ZIP8-iKO mice had a decreased abundance of fully glycosylated N-glycan species (26.6% in WT vs. 16.2% in ZIP8-iKO mice) and an increased abundance of truncated N-glycan species, especially under-galactosylated N-glycan species including monosialo-monogalacto-biantennary glycans (1.0% in WT vs. 3.7% in ZIP8-iKO mice), asialo-monogalacto-biantennary glycans (0 in WT vs 1.7% in ZIP8-iKO mice), and asialo-agalacto-biantennary glycans (0 in WT vs 1.4% in ZIP8-iKO mice). Similarly, compared with control mice, ZIP8-LSKO mice had a decreased abundance of fully glycosylated N-glycan species (41.0% in WT vs. 35.5% in ZIP8-LSKO mice) and an increased abundance of truncated N-glycan species, especially under-galactosylated N-glycan species monosialo-monogalacto-biantennary glycans (0.7% vs. 2.6%). Mn deficiency has also been found to moderately impair N-acetyl-glucosaminylation (32) mediated by another Mn-dependent glycosyltransferase, N-acetyl-glucosaminyltransferase II (33). In agreement with this, we found that ZIP8-iKO mice had reduced N-acetyl-glucosaminylation, as shown by an increased abundance of under–N-acetyl-glucosaminylated N-glycan species including monosialo-monogalacto-mono-GlcNAc-biantennary N-glycan (0 in WT vs. 0.8% in ZIP8-iKO mice) and asialo-agalacto-mono-GlcNAc-biantennary N-glycan (0 in WT vs. 1.5% in ZIP8-iKO mice). These patterns are consistent with reduced activity of the Mn-dependent enzymes β-1,4-galactosyltransferase and N-acetyl-glucosaminyltransferase II.

The lead variant in *SLC39A8* associated with lower whole-blood Mn levels and other pleiotropic traits is the coding variant rs13107325 (Ala391Thr), which is associated with lower hepatic *SLC39A8* expression (4, 6) and may encode a protein with reduced function (10, 11). We examined the N-glycan profile in the plasma of rs13107325 A391T homozygotes and matched major allele homozygotes. We detected the under-galactosylated N-glycan species monosialo-monogalacto-biantennary glycans in 58% of the minor allele homozygotes and only in 18% of the major allele homozygotes ($P = 0.049$). The abundance of monosialo-monogalacto-biantennary glycans was higher in the minor allele homozygotes than in the homozygous major allele carriers ($P = 0.047$; Figure 5E). These results indicate that homozygotes for the minor allele had reduced activity of the Mn-dependnent β-1,4-galactosyltransferase that was consistent with the association of the minor allele with lower blood Mn levels.
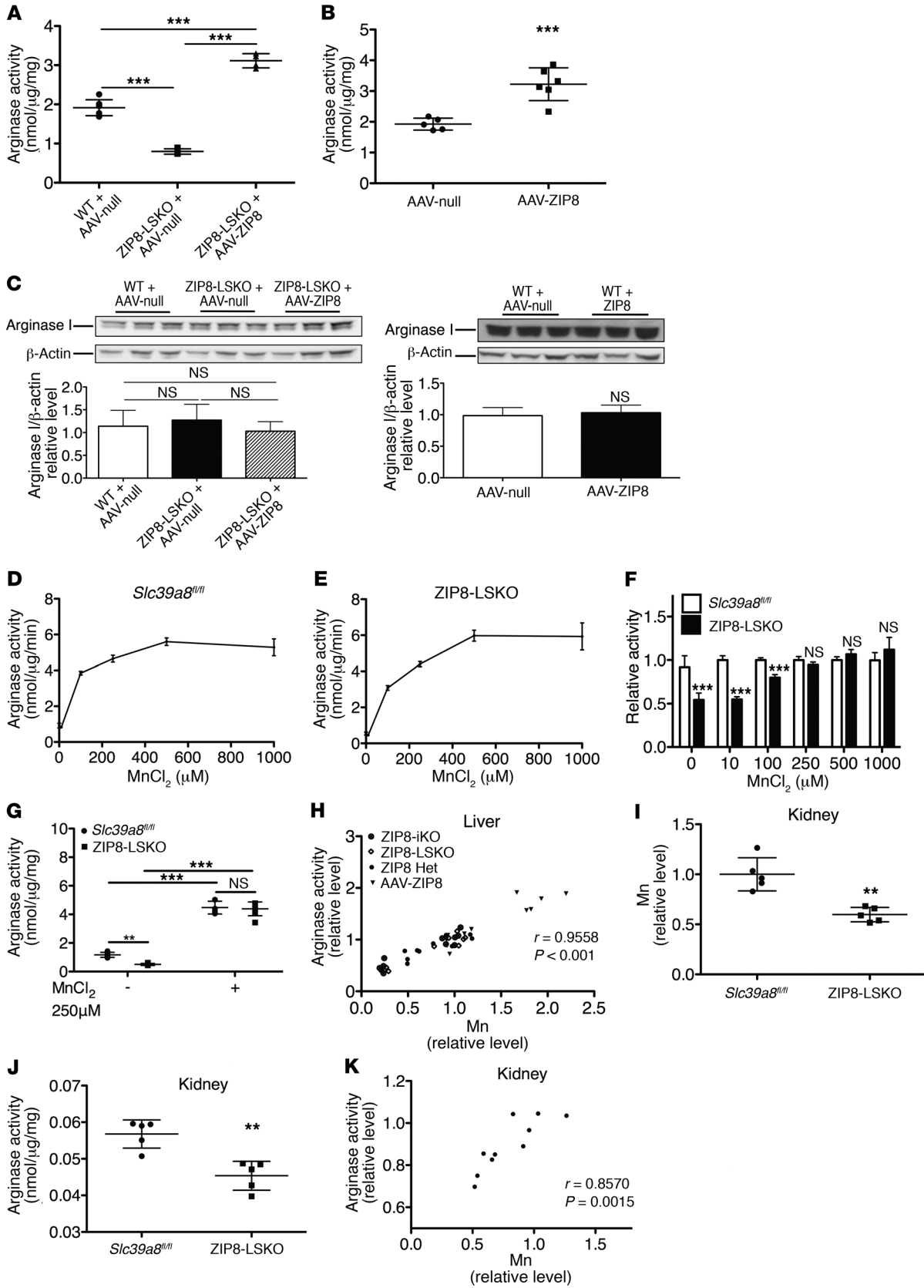
Figure 4. ZIP8 acts through Mn to quantitatively modulate arginase activity. (A) Arginase activity in the livers of 8- to 10-week-old male *Slc39a8*^fl/fl^ mice (WT) injected with AAV-null and ZIP8-LSKO mice injected with AAV-null or AAV-ZIP8 and sacrificed 4 weeks after injection (*n* = 7, 4, and 4, respectively). **(B)** Arginase activity in the livers of 10-week-old male B6 mice injected with AAV-null or AAV-ZIP8 and sacrificed 4 weeks after injection (*n* = 5 and 6, respectively). **(C)** Western blot analysis of arginase protein in the liver lysates of mice depicted in **A** and **B**. **(D** and **E)** Arginase activity in the livers of 10-week-old male *Slc39a8*^fl/fl^ and ZIP8-LSKO mice after preincubation with increasing concentrations of MnCl$_2$. Lysates from 3 mice of the same genotype were pooled, and 3 technical replicates were performed. **(F)** Arginase activity normalized to the average of the *Slc39a8*^fl/fl^ liver lysate at each MnCl$_2$ concentration. **(G)** Arginase activity in the livers of individual 10-week-old male *Slc39a8*^fl/fl^ and ZIP8-LSKO mice, with or without preincubation with 250 μM MnCl$_2$ (*n* = 6 and 7, respectively). **(H)** Correlation analysis of hepatic Mn levels and arginase activity in all 4 mouse models. Mn levels and arginase activity were normalized to the average of the control groups (*n* = 41). **(I)** ICP-OES analysis of kidney Mn levels in 10- to 12-week-old male *Slc39a8*^fl/fl^ and ZIP8-LSKO mice (*n* = 5). ICP-OES results were normalized to wet tissue weight. Mn levels were normalized to the average of the control group. **(J)** Arginase activity in the kidneys of mice described in **I** (*n* = 5). **(K)** Correlation analysis of kidney Mn levels and arginase activity in mice depicted in **I** and **J** (*n* = 10). Mn levels and arginase activity were normalized to the average of the control group. All data are shown as the mean ± SD. Comparisons between 2 groups were performed by Student's *t* test. Multiple comparisons in **A** were performed using 1-way ANOVA and Tukey's multiple comparisons test, and multiple comparisons in **G** were performed using 2-way ANOVA and Bonferroni's post-hoc test. ***$P \leq 0.001$, **$P \leq 0.01$. Correlation analyses were performed using Pearson's test.

Discussion

Our studies of the metal ion transporter ZIP8 were spurred by the observations that genetic variants, including a coding variant in the gene *SLC39A8*, are associated with whole-blood Mn levels (1) and multiple physiological traits (2–8). We used several *Slc39a8* loss-of-function and gain-of-function mouse models to gain insight into the role of ZIP8 in Mn metabolism and how it relates to Mn-dependent enzyme activity. Our studies revealed what we believe to be a novel role of hepatic ZIP8 in regulating whole-body Mn homeostasis, Mn-dependent enzymatic activity, and protein N-glycosylation. We discovered that hepatic ZIP8 regulates Mn metabolism in the liver, which in turn regulates Mn content in other organs and tissues, including kidney, brain, heart, and whole blood. We demonstrated that ZIP8 is localized to the hepatocyte canalicular membrane and functions to reclaim Mn from biliary excretion. We demonstrated that ZIP8 acts through Mn to modulate the activity of arginase, a Mn-dependent enzyme. We showed that ZIP8 deletion in mice led to defective protein N-glycosylation. Furthermore, we found that homozygosity for the minor allele of rs13107325 (Ala391Thr) in *SLC39A8*, which has reduced expression and protein function, is associated with hypogalactosylation. These findings are consistent with decreased activity of another Mn-dependent enzyme, β-1,4-galactosyltransferase. Therefore, our results demonstrate that hepatic ZIP8 regulates whole-body Mn homeostasis and Mn-dependent enzyme activity, providing potential insight into the association of genetic variants at the *SLC39A8* locus with physiological traits.

The lead variant at *SLC39A8* associated with whole-blood Mn levels and physiological traits is the coding variant rs13107325 (Ala391Thr), which has an 8% minor allele frequency in people of European ancestry (9). The substitution of a threonine for alanine at the 391 residue of ZIP8 is predicted to be damaging to ZIP8 function in silico and was experimentally shown to impair cellular Cd (10) and Zn (11) uptake by ZIP8. Rs13107325 is also an eQTL for *SLC39A8* in human liver and is associated with reduced expression (4, 6). Importantly, this variant associated with lower hepatic *SLC39A8* expression and reduced ZIP8 activity is associated with lower whole-blood Mn levels (1). Furthermore, *SLC39A8* loss-of-function mutations were recently identified in human patients with neurological and skeletal symptoms (16–18), and these patients were found to have decreased whole-blood Mn levels and reduced protein N-glycosylation, especially galacto-

sylation. Thus, the human data indicate that reduced expression and function of ZIP8 lead to reduced whole-blood Mn levels and protein N-glycosylation, especially galactosylation, a directionality fully consistent with our findings in *Slc39a8* loss-of-function mice and rs13107325 homozygous minor allele carriers.

One key finding of our study is the central role of ZIP8 in modulating biliary Mn excretion. DMT1 is believed to be the primary Mn transporter (24, 25), but it has been shown to be dispensable for Mn uptake in small intestine (34) and liver (24). The current model of Mn metabolism by the liver is that hepatocytes take up Mn from blood at the basolateral surface and excrete it into the bile at the apical surface. ZIP14, a close family member of ZIP8, may be responsible for the uptake of Mn from blood, as it has been reported to be localized on the basolateral membrane of hepatocytes (35) and has affinity for Mn in vitro (28, 36). Furthermore, patients carrying *SLC39A14* mutations showed excessive Mn accumulation in the whole blood and brain but a lack of Mn in the liver, possibly due to the bypassing of hepatic uptake by Mn and subsequent biliary excretion in the absence of *SLC39A14* (37). *SLC30A10*, a Mn exporter, is expressed in the liver and may be the transporter that excretes Mn from hepatocytes into the bile canaliculi (26). We have shown for the first time to our knowledge that ZIP8 is localized to the apical canalicular membrane of the hepatocyte and promotes the reuptake of Mn from the bile into the hepatocyte, thus acting to defend against Mn deficiency. Importantly, we showed that hepatic *Slc39a8* expression across a wide range, from homozygous knockout to overexpression, is quantitatively associated not only with hepatic Mn levels but also Mn levels in blood and multiple other tissues. Thus, our data indicate that hepatic ZIP8 is a quantitative regulator of whole-body Mn homeostasis. ZIP8-iKO mice do not have greater tissue reductions in Mn than do ZIP8-LSKO mice, suggesting that hepatic ZIP8 is the critical regulator of whole-body Mn homeostasis. Although ZIP8 has been detected in the proximal tubule cells of the kidney and is proposed to take up metal ions from the filtrate (28), we found that kidney Mn levels were not further decreased in ZIP8-iKO mice.

Mn deficiency caused by loss-of-function mutations of *SLC39A8* results in CDG II and mitochondrial disease, and there is great interest in determining whether Mn supplementation is a viable treatment for patients with CDG II (17, 18). Mn intoxication caused by occupational exposure (38), parenteral nutrition (30, 39), liver disease (40), and *SLC30A10* mutation (26) has
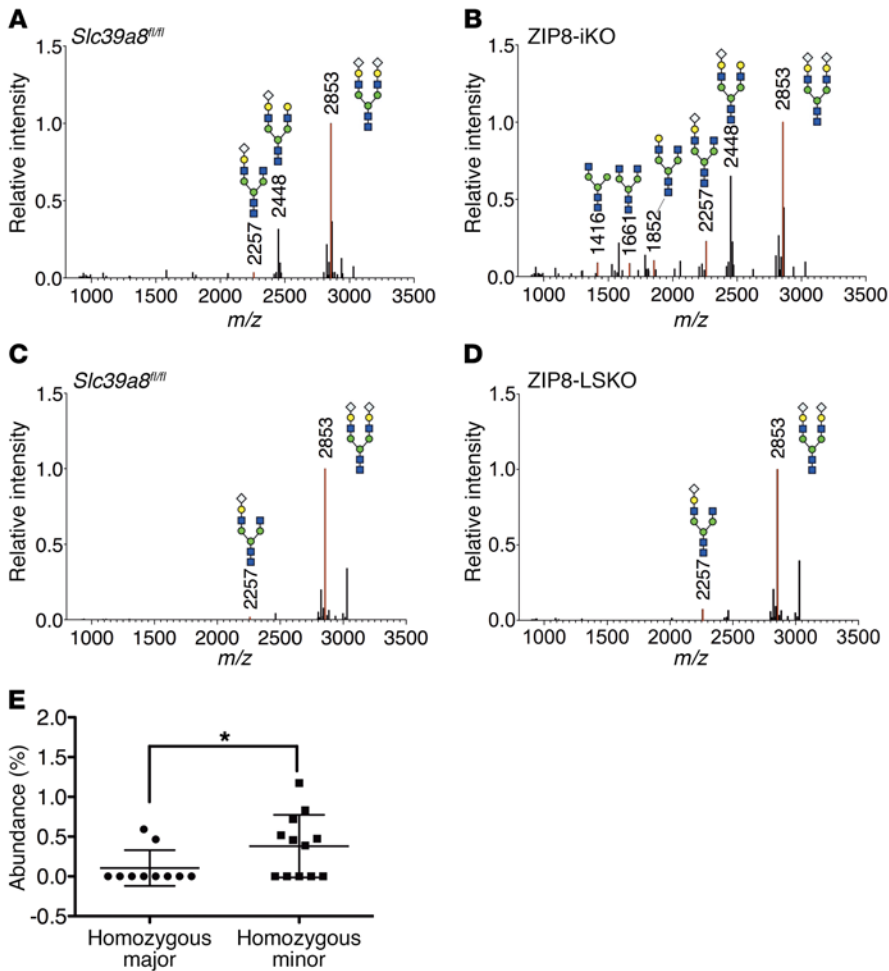
Figure 5. *Slc39a8* loss of function results in protein N-glycosylation defects. (**A** and **B**) MALDI-TOF analysis of the N-glycan profile for serum obtained 5 weeks after male *Slc39a8^fl/fl^* and ZIP8-iKO mice were injected with tamoxifen at 8 weeks of age. (**C** and **D**) MALDI-TOF analysis of the N-glycan profile for serum obtained from 10- to 12-week-old male *Slc39a8^fl/fl^* and ZIP8-LSKO mice. Each sample was pooled from 5 mice of the same genotype. White diamonds, sialic acid; yellow circles, galactose; blue squares, N-acetyl-glucosamine; green circles, mannose. The numbers above the peaks indicate the mass-to-charge ratios of the N-glycan species. 2853, disialo-biantennary glycans; 2448, monosialo-digalacto-biantennary glycans; 2257, monosialo-monogalacto-biantennary glycans; 1852, asialo-monogalacto-biantennary glycans; 1661, asialo-agalacto-biantennary glycans; 1416, asialo-agalacto-mono-GlcNAc-biantennary N-glycan. (**E**) Abundance of monosialo-monogalacto-biantennary glycans in the plasma of rs13107325 major and minor allele homozygotes. *N* = 11 and 12, respectively. Data are shown as the mean ± SD. Comparisons were performed using Student's *t* test. *$P \leq 0.05$.

been shown to cause manganism characterized by neurological and behavioral disorders resembling Parkinson's disease (27, 41). Our discovery that ZIP8 maintains whole-body Mn homeostasis by scavenging Mn from biliary excretion suggests that *SLC39A8* may be a therapeutic target for inhibition in the treatment of Mn intoxication and provides a rationale for Mn supplementation as a treatment of patients with *SLC39A8* mutations leading to CDG (*SLC39A8*-CDG).

Another key finding of our study is the dysregulation of Mn-dependent enzymes in *Slc39a8* loss-of-function mice. Arginase is known to be a Mn metalloenzyme, but the role of Mn in quantitatively regulating arginase activity has not been described in vivo. Our results indicate that Mn quantitatively modulates arginase activity over a wide range both below and above normal physiological levels. In addition, hepatic *Slc39a8* expression, by regulating whole-body tissue Mn levels, regulates arginase activity not only in the liver but in other tissues as well. Arginase inhibition has been shown to increase NO production, improve endothelial function, and decrease blood pressure (42–44). Therefore, our finding is consistent with the discovery in GWAS that the genetic variant associated with lower hepatic *SLC39A8* expression and reduced ZIP8 activity is associated with lower blood pressure. Further studies are needed to address this potential mechanism.

The Mn-dependent enzyme β-1,4-galactosyltransferase requires Mn for substrate binding and catalytic activity (22, 31). Mn deficiency

resulting from mutations of *SLC39A8* (17, 18) and *TMEM165* (32) have led to protein N-glycosylation defects, especially hypogalactosylation indicative of decreased β-1,4-galactosyltransferase activity. In addition, patients with *TMEM165* mutations (45) and *TMEM165* knocked down cells (32) have impaired N-acetyl-glucosaminylation, another protein N-glycosylation step mediated by the Mn-dependent glycosyltransferase N-acetyl-glucosaminyltransferase II. Our mice recapitulated the protein N-glycosylation defects resulting from Mn deficiency, including the hypogalactosylation seen in patients with *SLC39A8*-CDG (17) and patients with *TMEM165*-CDG as well as the hypo–N-acetyl-glucosaminylation seen in patients with *TMEM165*-CDG (45). In addition, we showed that hypogalactosylation is more common in rs13107325 A391T homozygous minor allele threonine carriers than in homozygous major allele alanine carriers, consistent with the association of the minor allele with decreased whole-blood Mn levels. Protein N-glycosylation affects the fate and function of proteins (46) and influences numerous physiological processes (19). In particular, it modulates the activity of key regulators of HDL-C metabolism (47–51) and has been implicated in dyslipidemia (48). Therefore, our findings suggest that protein N-glycosylation may be related to the association of *SLC39A8* with HDL-C and potentially other physiological traits in GWAS.

Patients carrying *SLC39A8* mutations had neurological and skeletal abnormalities that were evident very early in life (16–18). ZIP8-iKO and ZIP8-LSKO mice did not exhibit such abnormalities,

but we propose that the normal expression of *Slc39a8* during development and the postnatal timing of gene deletion in these mouse models may be the major explanation for this difference. In our experience, complete knockout of *Slc39a8* is not compatible with live births of knockout mice. Although *SLC39A8* variants are associated with HDL-C and BMI in GWAS, ZIP8-iKO and ZIP8-LSKO mice did not have overtly abnormal HDL-C levels or body weights on a chow or Western diet. More detailed investigation of these traits in our mouse models will be required. Finally, we are currently studying the blood pressure phenotype and potential regulatory mechanisms in ZIP8-iKO and ZIP8-LSKO mice.

Our study suggests a model in which hepatic expression of *SLC39A8* has systemic effects on Mn homeostasis, arginase activity, β-1,4-galactosyltransferase activity, and protein N-glycosylation. Hepatic ZIP8 scavenging of Mn from bile is the likely mechanism underlying the association of the *SLC39A8* locus with whole-blood Mn and the severe Mn deficiency in patients with *SLC39A8* mutations. The subsequent regulation of Mn-dependent enzymes may be related to the association of *SLC39A8* with other physiological traits in humans.

Methods

Animals. Mice harboring the *Slc39a8* conditional knockout allele C57BL/6-Slc39a8tm1.1 mrl and the constitutive knockout allele C57BL/6-Slc39a8tm1.2 mrl were provided by Merck. Details on the design of the ZIP8 mice can be found on the Taconic website (http://www.taconic.com/mouse-model/slc39a8-cko-11296 and http://www.taconic.com/mouse-model/slc39a8-ko). Briefly, the Slc39a8tm1.1 mrl allele has exon 3 flanked by loxP sites. The Slc39a8tm1.2 mrl allele was generated by Cre-mediated loxP site recombination, resulting in removal of the third exon of *Slc39a8*. The Slc39a8tm1.2 mrl allele deleted the N-terminal part of the ZIP domain and the first 2 transmembrane domains and generated a premature stop codon predicted to result in a protein null mouse. *Alb-Cre* mice, which express Cre under the control of the liver-specific albumin promoter beginning from P7, were obtained from The Jackson Laboratory (stock number 003574) and were crossed with C57BL/6-Slc39a8tm1.1 mrl mice to generate *Slc39a8* liver-specific knockout mice. ZIP8-iKO mice, which express Cre and the tamoxifen receptor ERT2 fusion protein under the control of the ubiquitin promoter, were obtained from The Jackson Laboratory (stock number 007001), crossed with C57BL/6-Slc39a8tm1.1 mrl mice, and injected with tamoxifen (100 mg/kg) for 5 consecutive days to generate an *Slc39a8*-inducible knockout. The Slc39a8tm1.1 mrl allele was detected by PCR using the following primers: 2476_27: 5′-CAGGGTTTCTCTGTGTAACAGG-3′; 2475_28: 5′-AGTGTACAGGCTCCAGCTACC-3′. Slc39a8tm1.2 mrl was detected by PCR using the following primers: 2476_27: 5′-CAGGGTTTCTCTGTGTAACAGG-3′ and 2475_32: 5′-CCAATATGGCCATAACAGATAGG-3′. The *Cre*-transgenic allele was detected by PCR using the following primers: 1011_1: Cre_tot1: 5′-ACGACCAAGTGACAGCAATG-3′ and 1011_2: Cre_tot2_5′-CTCGACCAGTTTAGTTACCC-3′. To make AAV8 virus for liver-specific human ZIP8 overexpression, *SLC39A8* cDNA was subcloned into a specialized AAV8 vector provided by the University of Pennsylvania Vector Core. This construct, together with a chimeric packaging construct in which the AAV2 rep gene was fused with the cap gene of AAV8, was used to produce AAV8 viral particles expressing human ZIP8 (AAV-ZIP8) at the University of Pennsylvania Vector Core.

AAV8 viral particles carrying an empty vector (AAV-null) were also produced by the University of Pennsylvania Vector Core. C57BL/6 mice were obtained from the The Jackson Laboratory and injected intraperitoneally with AAV-ZIP8 or AAV-null at a dose of 1×10^{11} genome copies per mouse. Experiments were performed 4 weeks after AAV injection.

Metal ion determination. Biliary and blood metals were measured using a PerkinElmer Elan 6100 ICP-MS System (inductively coupled plasma MS system) at the Pennsylvania Animal Diagnostic Laboratory System (PADLS), New Bolton Center Toxicology Laboratory of the University of Pennsylvania School of Veterinary Medicine, as previously described (52). For each bile sample, bile from 2 animals was combined, and weight and volume were recorded before measurement. For each measurement, the sample was digested overnight with twice the amount (weight/volume) of 70% nitric acid at 70°C, and 0.15 ml of the digested sample was diluted with deionized water to a final volume of 5 ml for analysis. The concentration was measured using a calibration curve of aqueous standards prepared at 4 different concentrations of each metal. The results were reported in parts per million (ppm) on the basis of weight. Concentrations were calculated by dividing the total amount by the volume.

Metals in the liver, kidney, brain, heart, and small intestine were measured using a SPECTRO ICP-OES (inductively coupled plasma optical emission spectrometry) system at the Department of Earth and Environmental Science of the School of Arts and Sciences of the University of Pennsylvania, as previously described (53). Samples were weighted, digested with 800 μl HNO$_3$/HCl [3:1] at 70°C overnight, and diluted to a final volume of 2.5 ml for analysis. The concentration was measured using a calibration curve of aqueous standards prepared at 5 different concentrations of each metal. The results were reported in ppm on the basis of volume. The total amount, determined by multiplying the concentration with the volume, was divided by the wet weight of the tissue to obtain the metal amount per milligram of the tissue.

^{54}*Mn uptake study.* HEK293T cells were seeded in 24-well plates and transfected using Lipofectamine 2000 (Invitrogen, Thermo Fisher Scientific) the next day at a density of approximately 80% confluence. Twenty-four hours after transfection, the cells were washed once with HBSS (Ca^{2+}, Mg^{2+}-free) and incubated with prewarmed uptake buffers at 37°C for 15 minutes. The uptake buffers contained different concentrations of MnCl$_2$ prepared by diluting MnCl$_2$ (10 μM, 4 μci/ml) 1, 1.3, 2, 4, 10, and 40 times. The 15-minute time point had been shown by a pilot study to be within the linear phase of Mn uptake by ZIP8. To terminate the uptake, the uptake buffer was removed and the cells washed 3 times with cold HBSS (Ca^{2+}, Mg^{2+}-free). Five hundred microliters of NaOH (1 mM) was added into each well to digest the cells. At least 2 hours later, 300 μl cell lysate was removed for liquid scintillation counting, and 50 μl was used for protein measurement by bicinchoninic acid (BCA) assay.

Arginase activity assay. An arginase activity assay was performed as previously described (54), with slight modifications. In brief, approximately 50 mg liver was homogenized in 4× volume of PBS with protease and phosphatase inhibitors. Lysate was centrifuged at 4°C at 14,000 ×*g* for 15 minutes. The supernatant was further diluted by 30-fold and used in the arginase activity and BCA assays. For the arginase activity assay without MnCl$_2$ activation, 50 μl diluted supernatant was incubated with 220 μl glycine-NaOH buffer (pH 9.6) and 100 μl arginine (68 mM, pH 9.6) at 37°C for 10 minutes, which a pilot experiment had shown to be within the linear phase of urea production. For the arginase activity assay with MnCl$_2$, 50 μl diluted supernatant, either pooled

or from an individual animal, was first incubated with 20 μl MnCl$_2$ of the desired concentration and 200 μl glycine-NaOH buffer (pH 9.6) at 55°C for 10 minutes. After cooling down, 100 μl arginine was added, and the sample was incubated at 37°C for 10 minutes. Nine hundred microliters H$_2$SO$_4$/H$_3$PO$_4$/H$_2$O (1:3:7) was added to stop the reaction. Forty microliters α-isonitrosopropiophenone (9%) dissolved in ethanol was added, and the sample was heated at 95°C for 30 minutes to develop color. After cooling down in the dark, 200 μl of the sample was transferred to a 96-well plate, and the color was quantified using a plate reader at 540 nm. Urea solutions with known concentrations (10 mM, 5 mM, 2.5 mM, 1.25 mM, and 0.625 mM) were used to produce a standard curve. Sample urea production was calculated on the basis of the standard curve and normalized to protein content measured by BCA assay. Arginase activity was determined by the amount of urea produced per microgram protein in 1 minute.

N-glycan profile analysis. Serum or plasma N-glycan profile analysis was performed as previously described (55). In brief, samples were digested with PNGase F at 37°C overnight to release N-glycans from total glycoproteins. The released N-glycans were purified with a C18 column followed by a carbograph column. The purified N-glycans were permethylated by a traditional liquid-liquid permethylation method and desalted by organic extraction with chloroform and water. Finally, permethylated N-glycan sodium adducts were analyzed by MALDI-TOF-MS to obtain N-glycan profiles. The percentage of total abundance of a glycan species corresponding to a peak in the chromatogram was calculated by dividing the area under the peak by the area under all of the peaks.

Immunoblot analysis. Liver lysate supernatant was prepared as described in the arginase activity assay. Protein (50 μg) was separated using the NuPage SDS Page System (Invitrogen, Thermo Fisher Scientific). The following primary antibodies were used: anti-ZIP8 (1:1,000; Proteintech; 20459-1-AP); anti–arginase I (1:2,500; BD Biosciences; 610708); and anti–β actin (1:1,000; Santa Cruz Biotechnology Inc.; sc-81178). HRP-conjugated anti-rabbit (catalog NA934V) and anti-mouse secondary antibodies (catalog NA931V) (1:2,500; GE Healthcare Life Sciences) and the Classico ECL Reagent (EMD Millipore) were used to visualize the signal.

Immunofluorescence. Liver pieces were frozen in OCT and cut into 8-μm-thick sections at the Histology and Gene Expression Core of the Cardiovascular Institute of the University of Pennsylvania. Immunofluorescence was performed at the Histology and Gene Expression Core using the following antibodies: anti-ZIP8 (1:50; Sigma-Aldrich; HPA038832) and anti-MDR (C-19) (1:2,500; Santa Cruz Biotechnology Inc.; sc-1517).

qPCR. RNA was isolated using TRIzol (Thermo Fisher Scientific), and cDNA was made using a High Capacity cDNA Reverse Tran-

scription Kit (Applied Biosystems). Fast SYBR Green Mastermix (Life Technologies, Thermo Fisher Scientific; 4385614) was used for qPCR analysis. The SYBR primers used were as follows: *Slc39a8*, forward: 5′-CAACGCAAAGCCCAGTCTTT-3′; *Slc39a8*, reverse: 5′-GCGTTT-GAGAAAAGAGTCCCAA-3′; *SLC39A8*, forward: 5′-TTCCAGAGG-CATTTGGATTT-3′; *SLC39A8*, reverse: 5′-GGGTATGACCATTCT-GACCAT-3′; *Gapdh*, forward: 5′-TGTGTCCGTCGTGGATCTGA-3′; and *Gapdh*, reverse: 5′-CCTGCTTCACCACCTTCTTGAT-3′.

Statistics. Comparisons of 2 samples were performed using the 2-tailed Student's *t* test. Multiple comparisons were performed using 1-way ANOVA and Tukey's multiple comparisons test. Multiple comparisons of different treatments were done using 2-way ANOVA and Bonferroni's multiple comparisons test. Comparison of the frequency of the truncated N-glycan was performed using the χ^2 test. Correlation analyses were performed using Pearson's test. A *P* value of less than 0.05 was considered statistically significant.

Study approval. All animal experiments were reviewed and approved by the IACUC of the University of Pennsylvania.

Author contributions

DJR and WL conceived the hypothesis, designed and interpreted the experiments, and wrote the manuscript; WL performed the experiments; NJH supervised experiments, helped interpret the results, and edited the manuscript; DRV assisted with the ICP-OES experiment and data analysis; XL performed the N-glycan profiling experiment; PTD and GL provided technical help; MH provided intellectual input regarding the N-glycan profiling experiment and helped interpret the results; and TW, RS, and ER provided intellectual input.

Acknowledgments

Address correspondence to: Daniel J. Rader, Smilow Center for Translational Research, SCTR 11-125, 3400 Civic Center Boulevard, Philadelphia, Pennsylvania 19104-5158, USA. Phone: 215.573.4176; E-mail: rader@mail.med.upenn.edu.

1. Ng E, et al. Genome-wide association study of toxic metals and trace elements reveals novel associations. *Hum Mol Genet*. 2015;24(16):4739–4745.
2. International Consortium for Blood Pressure Genome-Wide Association Studies, et al. Genetic variants in novel pathways influence blood pressure and cardiovascular disease risk. *Nature*. 2011;478(7367):103–109.
3. Ehret GB, et al. The genetics of blood pressure regulation and its target organs from association studies in 342,415 individuals. *Nat Genet*. 2016;48(10):1171–1184.
4. Teslovich TM, et al. Biological, clinical and population relevance of 95 loci for blood lipids. *Nature*. 2010;466(7307):707–713.
5. Global Lipids Genetics Consortium, et al. Discovery and refinement of loci associated with lipid levels. *Nat Genet*. 2013;45(11):1274–1283.
6. Speliotes EK, et al. Association analyses of 249,796 individuals reveal 18 new loci associated with body mass index. *Nat Genet*. 2010;42(11):937–948.
7. Carrera N, et al. Association study of nonsynonymous single nucleotide polymorphisms in schizo-
phrenia. *Biol Psychiatry*. 2012;71(2):169–177.
8. Schizophrenia Working Group of the Psychiatric Genomics Consortium. Biological insights from 108 schizophrenia-associated genetic loci. *Nature*. 2014;511(7510):421–427.
9. Reference SNP (refSNP) Cluster Report: rs13107325. NCBI. https://www.ncbi.nlm.nih.gov/projects/SNP/snp_ref.cgi?rs=13107325. Accessed May 2, 2017.
10. Zhang R, et al. A blood pressure-associated variant of the SLC39A8 gene influences cellular cadmium accumulation and toxicity. *Hum Mol Genet*.

2016;25(18):4117–4126.

11. Marger L, Bertrand D, Singec I, Xi HS, Wendland JR, Schubert CR. Functional characterization of ZiP8, a zinc transporter with potential relevance for neuropsychiatric disorders. HiQScreen. http://www.hiqscreen.com/Posters/Poster Zip8%20CRS.pdf. Accessed March 24, 2017.

12. Begum NA, Kobayashi M, Moriwaki Y, Matsumoto M, Toyoshima K, Seya T. Mycobacterium bovis BCG cell wall and lipopolysaccharide induce a novel gene, BIGM103, encoding a 7-TM protein: identification of a new protein family having Zn-transporter and Zn-metalloprotease signatures. *Genomics*. 2002;80(6):630–645.

13. He L, et al. ZIP8, member of the solute-carrier-39 (SLC39) metal-transporter family: characterization of transporter properties. *Mol Pharmacol*. 2006;70(1):171–180.

14. Wang CY, et al. ZIP8 is an iron and zinc transporter whose cell-surface expression is upregulated by cellular iron loading. *J Biol Chem*. 2012;287(41):34032–34043.

15. Gálvez-Peralta M, et al. ZIP8 zinc transporter: indispensable role for both multiple-organ organogenesis and hematopoiesis in utero. *PLoS One*. 2012;7(5):e36055.

16. Boycott KM, et al. Autosomal-Recessive Intellectual Disability with Cerebellar Atrophy Syndrome Caused by Mutation of the Manganese and Zinc Transporter Gene SLC39A8. *Am J Hum Genet*. 2015;97(6):886–893.

17. Park JH, et al. SLC39A8 Deficiency: A Disorder of Manganese Transport and Glycosylation. *Am J Hum Genet*. 2015;97(6):894–903.

18. Riley LG, et al. A SLC39A8 variant causes manganese deficiency, and glycosylation and mitochondrial disorders. *J Inherit Metab Dis*. 2017;40(2):261–269.

19. Scott K, Gadomski T, Kozicz T, Morava E. Congenital disorders of glycosylation: new defects and still counting. *J Inherit Metab Dis*. 2014;37(4):609–617.

20. Wedler FC. Biochemical and nutritional role of manganese: an overview. In: Klimis-Tavntzis DJ, ed. *Manganese in health and disease*. Boca Raton, FL: CRC Press, Inc. 1994;1–37.

21. Kanyo ZF, Scolnick LR, Ash DE, Christianson DW. Structure of a unique binuclear manganese cluster in arginase. *Nature*. 1996;383(6600):554–557.

22. Ramakrishnan B, Ramasamy V, Qasba PK. Structural snapshots of beta-1,4-galactosyltransferase-I along the kinetic pathway. *J Mol Biol*. 2006;357(5):1619–1633.

23. Keen CL, et al. Nutritional aspects of manganese from experimental studies. *Neurotoxicology*. 1999;20(2-3):213–223.

24. Chua AC, Morgan EH. Manganese metabolism is impaired in the Belgrade laboratory rat. *J Comp Physiol B, Biochem Syst Environ Physiol*. 1997;167(5):361–369.

25. Chen P, Parmalee N, Aschner M. Genetic factors and manganese-induced neurotoxicity. *Front Genet*. 2014;5:265.

26. Quadri M, et al. Mutations in SLC30A10 cause parkinsonism and dystonia with hypermanganesemia, polycythemia, and chronic liver disease. *Am J Hum Genet*. 2012;90(3):467–477.

27. Roth JA. Homeostatic and toxic mechanisms regulating manganese uptake, retention, and elimination. *Biol Res*. 2006;39(1):45–57.

28. Fujishiro H, Yano Y, Takada Y, Tanihara M, Himeno S. Roles of ZIP8, ZIP14, and DMT1 in transport of cadmium and manganese in mouse kidney proximal tubule cells. *Metallomics*. 2012;4(7):700–708.

29. Davis CD, Zech L, Greger JL. Manganese metabolism in rats: an improved methodology for assessing gut endogenous losses. *Proc Soc Exp Biol Med*. 1993;202(1):103–108.

30. Aschner JL, Aschner M. Nutritional aspects of manganese homeostasis. *Mol Aspects Med*. 2005;26(4-5):353–362.

31. Ramakrishnan B, Boeggeman E, Ramasamy V, Qasba PK. Structure and catalytic cycle of beta-1,4-galactosyltransferase. *Curr Opin Struct Biol*. 2004;14(5):593–600.

32. Potelle S, et al. Glycosylation abnormalities in Gdt1p/TMEM165 deficient cells result from a defect in Golgi manganese homeostasis. *Hum Mol Genet*. 2016;25(8):1489–1500.

33. Bendiak B, Schachter H. Control of glycoprotein synthesis. Kinetic mechanism, substrate specificity, and inhibition characteristics of UDP-N-acetylglucosamine:alpha-D-mannoside beta 1-2 N-acetylglucosaminyltransferase II from rat liver. *J Biol Chem*. 1987;262(12):5784–5790.

34. Shawki A, et al. Intestinal DMT1 is critical for iron absorption in the mouse but is not required for the absorption of copper or manganese. *Am J Physiol Gastrointest Liver Physiol*. 2015;309(8):G635–G647.

35. Nam H, et al. ZIP14 and DMT1 in the liver, pancreas, and heart are differentially regulated by iron deficiency and overload: implications for tissue iron uptake in iron-related disorders. *Haematologica*. 2013;98(7):1049–1057.

36. Girijashanker K, et al. Slc39a14 gene encodes ZIP14, a metal/bicarbonate symporter: similarities to the ZIP8 transporter. *Mol Pharmacol*. 2008;73(5):1413–1423.

37. Tuschl K, et al. Mutations in SLC39A14 disrupt manganese homeostasis and cause childhood-onset parkinsonism-dystonia. *Nat Commun*. 2016;7:11601.

38. Roels H, et al. Epidemiological survey among workers exposed to manganese: effects on lung, central nervous system, and some biological indices. *Am J Ind Med*. 1987;11(3):307–327.

39. Reimund JM, Dietemann JL, Warter JM, Baumann R, Duclos B. Factors associated to hypermanganesemia in patients receiving home parenteral nutrition. *Clin Nutr*. 2000;19(5):343–348.

40. Hauser RA, Zesiewicz TA, Rosemurgy AS, Martinez C, Olanow CW. Manganese intoxication and chronic liver failure. *Ann Neurol*. 1994;36(6):871–875.

41. Chen P, Chakraborty S, Peres TV, Bowman AB, Aschner M. Manganese-induced Neurotoxicity: From C. elegans to Humans. *Toxicol Res (Camb)*. 2015;4(2):191–202.

42. Chicoine LG, Paffett ML, Young TL, Nelin LD. Arginase inhibition increases nitric oxide production in bovine pulmonary arterial endothelial cells. *Am J Physiol Lung Cell Mol Physiol*. 2004;287(1):L60–L68.

43. Shatanawi A, et al. Angiotensin II-induced vascular endothelial dysfunction through RhoA/Rho kinase/p38 mitogen-activated protein kinase/arginase pathway. *Am J Physiol, Cell Physiol*. 2011;300(5):C1181–C1192.

44. Holowatz LA, Kenney WL. Up-regulation of arginase activity contributes to attenuated reflex cutaneous vasodilatation in hypertensive humans. *J Physiol (Lond)*. 2007;581(Pt 2):863–872.

45. Xia B, et al. Serum N-glycan and O-glycan analysis by mass spectrometry for diagnosis of congenital disorders of glycosylation. *Anal Biochem*. 2013;442(2):178–185.

46. Moremen KW, Tiemeyer M, Nairn AV. Vertebrate protein glycosylation: diversity, synthesis and function. *Nat Rev Mol Cell Biol*. 2012;13(7):448–462.

47. Skropeta D, et al. N-Glycosylation regulates endothelial lipase-mediated phospholipid hydrolysis in apoE- and apoA-I-containing high density lipoproteins. *J Lipid Res*. 2007;48(9):2047–2057.

48. van den Boogert MA, et al. Genetic defects inprotein glycosylation as a cause of dyslipidemia [abstract 14741]. *Circulation*. 2013;128(Suppl 22):A14741.

49. Albers JJ, Day JR, Wolfbauer G, Kennedy H, Vuletic S, Cheung MC. Impact of site-specific N-glycosylation on cellular secretion, activity and specific activity of the plasma phospholipid transfer protein. *Biochim Biophys Acta*. 2011;1814(7):908–911.

50. Viñals M, Xu S, Vasile E, Krieger M. Identification of the N-linked glycosylation sites on the high density lipoprotein (HDL) receptor SR-BI and assessment of their effects on HDL binding and selective lipid uptake. *J Biol Chem*. 2003;278(7):5325–5332.

51. Singaraja RR, et al. Specific mutations in ABCA1 have discrete effects on ABCA1 function and lipid phenotypes both in vivo and in vitro. *Circ Res*. 2006;99(4):389–397.

52. Stout JD, Brinker DF, Driscoll CP, Davison S, Murphy LA. Serum biochemistry values, plasma mineral levels, and whole blood heavy metal measurements in wild northern goshawks (Accipiter gentilis). *J Zoo Wildl Med*. 2010;41(4):649–655.

53. Murty S, et al. Nanoparticles functionalized with collagenase exhibit improved tumor accumulation in a murine xenograft model. *Part Part Syst Charact*. 2014;31(12):1307–1312.

54. Corraliza IM, Campo ML, Soler G, Modolell M. Determination of arginase activity in macrophages: a micromethod. *J Immunol Methods*. 1994;174(1-2):231–235.

55. Li X, Raihan MA, Reynoso FJ, He M. Glycosylation analysis for congenital disorders of glycosylation. *Curr Protoc Hum Genet*. 2015;86:17.18.1–17.18.22.